Available online at www.sciencedirect.com

ScienceDirect

Acta Materialia 61 (2013) 6790–6801

Acta MATERIALIA

www.elsevier.com/locate/actamat

Twinning stress in shape memory alloys: Theory and experiments

J. Wang, H. Sehitoglu *

Department of Mechanical Science and Engineering, University of Illinois at Urbana-Champaign, 1206 West Green Street, Urbana, IL 61801, USA

Received 8 May 2013; received in revised form 21 July 2013; accepted 26 July 2013
Available online 23 August 2013

Abstract

Utilizing first-principles atomistic simulations we present a twin nucleation model based on the Peierls–Nabarro formulation. We investigated twinning in several important shape memory alloys, starting with Ni_2FeGa (14M modulated monoclinic and $L1_0$ crystals) to illustrate the methodology, and predicted the twin stress in Ni_2MnGa, NiTi, Co_2NiGa, and Co_2NiAl martensites, all of which were in excellent agreement with the experimental results. Minimization of the total energy led to determination of the twinning stress accounting for the twinning energy landscape in the presence of interacting multiple twin dislocations and disregistry profiles at the dislocation core. The validity of the model was confirmed by determining the twinning stress from experiments on Ni_2FeGa (14M and $L1_0$), NiTi, and Ni_2MnGa and utilizing results from the literature for Co_2NiGa and Co_2NiAl martensites. This paper demonstrates that the predicted twinning stress can vary from 3.5 MPa in 10M Ni_2MnGa to 129 MPa for the B19′ NiTi case, consistent with the experimental results.

Keywords: Twinning stress; Twin nucleation model; Peierls–Nabarro; Shape memory alloys; Atomistic simulations

1. Introduction

To facilitate the design of new transforming alloys, including those proposed for magnetic shape memory, twinning modes associated with these alloys need to be fully understood [1]. The objective of the current paper was to study the most important twin modes in monoclinic and tetragonal (modulated and non-modulated) shape memory martensites and establish their twin fault energy barriers that are in turn utilized to predict the twinning stress. A new model for twin nucleation is proposed which shows excellent overall agreement with the experimental results.

Martensite twinning and subsequent recovery upon heating is called the "shape memory effect" [2]. In the "shape memory" case, when the internally twinned martensite is subsequently deformed the twin variants that are oriented favorably to the external stress grow at the expense of the others. The growth of the twin is a process of advancement of twin interfaces and requires overcoming an energy barrier called the "unstable twin fault energy" [3,4]. Upon unloading the twinning-induced deformation remains. If the material is heated above the austenite finish temperature the material reverts back to austenite. Hence, heating and cooling changes can make the material behave as an actuator, which is termed the "shape memory effect". In this paper we present experimental results of twinning stress for several important shape memory alloys and compare the results with theory.

It is now well known that the phenomenon of twinning during shape memory processes relies on complex atomic movements in the martensitic crystal. Despite the significant importance of twinning in shape memory alloys (SMAs), there have been limited attempts to develop models to predict the twinning stress from first principles. The twinning energy landscapes for ordered binary and ternary alloys are more complex compared with pure face-centered cubic (fcc) metals [5–7]. Thus a fundamental understanding of twin nucleation is essential to capture the mechanical response of SMAs. This is the subject of this paper.

* Corresponding author. Tel.: +1 2173334112.
E-mail address: huseyin@illinois.edu (H. Sehitoglu).

1359-6454/$36.00
http://dx.doi.org/10.1016/j.actamat.2013.07.053

Several methodologies exist to evaluate the twin nucleation and migration stresses of materials [4,8–12]. However, the early models either require one or more fitting parameters or depend only on the intrinsic stacking fault energy γ_{isf}, and they predict unrealistically high twinning stresses. The Peierls–Nabarro (P–N) formalism can be utilized for rapid assessment of the deformation behavior of binary and ternary shape memory materials and to evaluate different crystal structures of martensites. A brief description of the P–N model used to predict the Peierls stress is given in the Appendix. The formalism for dislocation slip stress determination utilizing the P–N concepts is well established, while twinning stress determination is not as well developed. If a P–N based twinning model was developed then it could lead to a quantitative prediction of twinning stress in SMAs, and a better understanding of the factors that govern the shape memory effect. The current study addresses this important issue.

Martensite can undergo twinning deformation associated with the shape memory effect, as explained earlier. The stress levels for martensite twinning can be determined from experiments at temperatures below the martensite finish temperature. Fig. 1 shows a schematic of the stress–strain curve of Ni_2FeGa at a temperature below the martensite finish temperature. During loading twin interfaces advance in 14M (modulated monoclinic structure), followed by twinning of the $L1_0$ structure at higher strains. As we show later, these two crystal structures of Ni_2FeGa have distinctly different twin stresses. Upon unloading the detwinned martensitic structure remains, which is recovered upon heating above the austenite finish temperature.

From our previous tests we noted that compressive loading experiments are better suited to avoid premature fracture in tension [13]. When the specimen is deformed the martensite twinning process initiates at a finite stress level. There are very limited experiments in the literature on the martensite twinning stress of ferromagnetic shape memory alloys such as Ni_2FeGa, Co_2NiAl and Co_2NiGa. There have been more experiments on NiTi and Ni_2MnGa. The research teams of Sehitoglu and Chumlyakov have conducted experiments below the martensite finish temperature on a number of advanced shape memory alloys [14,15]. Since the twin thicknesses are on the nano scale it is difficult to experimentally observe the onset of twinning in situ. Additionally, several twin systems can co-exist, hence making it rather complicated to experimentally discern the twin stress when multiple systems interact, such as in NiTi and Ni_2FeGa. Therefore, theoretical calculations provide considerable insight.

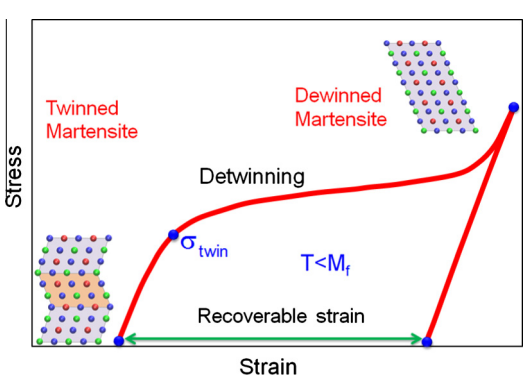

Fig. 1. Schematic stress–strain curve showing the detwinning of internally twinned martensite (multiple variant) to detwinned martensite (single crystal) Ni_2FeGa at low temperature. Upon unloading plastic strain is observed in the material, which can be fully recovered upon heating.

On the meso scale our current treatment deals with the dislocation movements leading to twin formation. Several modifications to the original P–N treatment were implemented in the course of the study. On the atomic scale, during calculation of the generalized planar fault energy (GPFE) curve full internal atom relaxation was allowed. This allows a three-dimensional description of the energy landscape with displacements in two other directions in addition to the imposed shear. The misfit energy expression accounts for the discreteness in the lattice across atomic pairs and is not treated as a continuous integral. This energy description is dependent on the spacing between two adjacent twinning partials and results in a more realistic twin stress evaluation. Both of these modifications enrich the original approach put forward by Peierls and Nabarro. A further advancement forwarded in this study is to incorporate the elastic strain fields in the overall energy expression accounting for the mutual interaction of dislocation fields. Upon minimization of the total energy we seek the critical twin nucleation stress. We show results for Ni_2FeGa in comparison with our experiments, but the methodology developed is appealing and was applied to other materials. The outcome of these calculations is that one can evaluate magnitudes of critical twin nucleation stress in better agreement with the experimental results. The proposed twin nucleation model can be used for rapid and accurate prediction of twin stresses of potential shape memory alloys before undertaking costly experimental programs.

2. Methodologies for twin nucleation

We model the deformation process of twin nucleation at the atomic level and integrate this with a mesoscale description of the overall energy. On the atomic level the twinning energy landscape (GPFE) is established representing the lattice shearing process due to the passage of twinning partials [12]. On the mesoscale level an extended P–N formulation is proposed to determine the twin configuration and address the total energy associated with twin nucleation.

2.1. Density functional theory (DFT) calculation set-up

The GPFE provides a comprehensive description of twins, which is the energy per unit area required to form n layer twins by shearing n consecutive layers along the twinning direction [12]. The first-principles total energy

calculations were carried out using the Vienna Ab initio Simulation Package (VASP) with the projector augmented wave (PAW) method and the generalized gradient approximation (GGA) [16,17]. Monkhorst Pack $9 \times 9 \times 9$ k-point meshes were used for the Brillouin zone integration to ensure the convergence of results. An energy cut-off of 500 eV was used for the plane wave basis set. The total energy was converged to less than 10^{-5} eV per atom. Periodic boundary conditions across the supercell were used to represent the bulk material. We have used an L layer based cell to calculate fault energies to generate a GPFE curve for a particular system. We assessed the convergence of the GPFE energies with respect to increasing L, which indicates that the fault energy interaction in adjacent cells due to periodic boundary conditions will be negligible. Convergence is ensured once the energy calculations for the L and $L+1$ layers yield the same GPFE. For each shear displacement u full internal atom relaxation, including in the perpendicular and parallel directions to the fault plane, was allowed to minimize the short-range interactions between misfitted layers near to the fault plane. During the shear deformation process the volume of the supercell was maintained constant, ensuring the correct twin structure [18,19]. This relaxation process caused a small additional atomic displacement r ($r = \sqrt{r_x + r_y + r_z}$) within 1% in magnitude of the Burgers vector **b**. Thus the total fault displacement is not exactly equal to u but involves additional r. The total energy of the deformed (faulted) crystal was minimized during this relaxation process, which avoids atoms coming too close to each other during shear [20–22]. From the calculated results for deformation twinning we note that the energy barrier after full relaxation was nearly 10% lower than the barrier when relaxation only perpendicular to the fault plane was allowed.

2.2. Twinning energy landscapes (GPFE): the $L1_0$ Ni_2FeGa example

The deformation twinning system $\langle 1\,1\,\bar{2}\rangle\{1\,1\,1\}$ has been experimentally observed for the $L1_0$ structure in past works [23–28], the same as that of fcc metals. In this study we conducted simulations to determine the GPFE of $L1_0$ Ni_2FeGa by successive shearing every (1 1 1) plane over a $1/6[1\,1\,\bar{2}]$ dislocation. We noted that the formation of twin system $1/6[1\,1\,\bar{2}](1\,1\,1)$ of $L1_0$ Ni_2FeGa requires no additional atomic shuffling, which was also observed for other $L1_0$ structures [24,29–31] and fcc materials [4,12,32–34]. Fig. 2 shows the $L1_0$ face-centered tetragonal (fct) structure with corresponding lattice parameters $a = b = 3.68$ Å and $c = 3.49$ Å. We note that the tetragonal axis is $2c$, so the $L1_0$ unit cell contains two fct unit cells. These lattice parameters are in a good agreement with experimental measurements [35]. These precisely determined lattice parameters form the foundation of atomistic simulations to establish the GPFE. The twinning plane (1 1 1) and the $[1\,1\,\bar{2}]$ direction in $L1_0$ Ni_2FeGa are shaded violet and denoted by the red arrow in Fig. 2. We note that if the

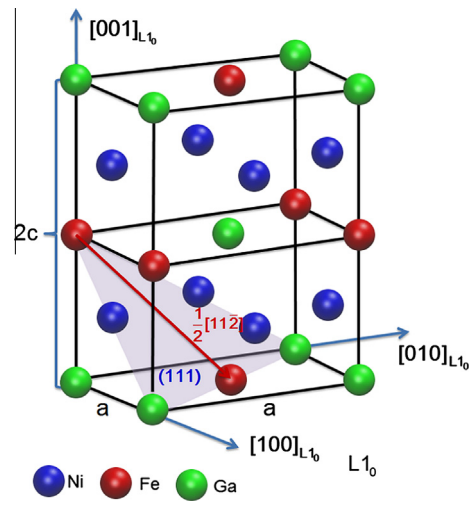

Fig. 2. $L1_0$ structure and twinning system of Ni_2FeGa. The $L1_0$ fct structure with lattice parameters a, a and $2c$ contains two fct unit cells. The twining plane (1 1 1) is shaded violet and direction $[1\,1\,\bar{2}]$ by a red arrow. The blue, red and green atoms correspond to Ni, Fe and Ga atoms, respectively. (For interpretation of the references to color in this figure legend, the reader is referred to the web version of this article.)

tetragonal axis is taken to be c, not $2c$, the corresponding twinning plane will be (1 1 2).

Fig. 3 shows a top view from the direction perpendicular to the (1 1 1) twinning plane with three layers of atoms stacking in $L1_0$ Ni_2FeGa. Different sizes of atoms represent three successive (1 1 1) layers. The twinning partial dislocation is $1/6[1\,1\,\bar{2}]$ (Burgers vector $\mathbf{b} = 1.45$ Å) and is shown by a red arrow.

We conducted simulations to determine the GPFE of $L1_0$ Ni_2FeGa by successive shear of every (1 1 1) plane over a $1/6[1\,1\,\bar{2}]$ partial dislocation. Fig. 4a shows the perfect $L1_0$ lattice of Ni_2FeGa, while Fig. 4b is the lattice with a three layer twin after shear displacement u (shown by the red arrow) in successive (1 1 1) planes (the twinning plane

Fig. 3. Schematic top view from the direction perpendicular to the (1 1 1) twinning plane in $L1_0$ Ni_2FeGa. Different sizes of atoms represent three successive (1 1 1) layers. Twinning partial $1/6[1\,1\,\bar{2}]$ is shown by a red arrow. (For interpretation of the references to color in this figure legend, the reader is referred to the web version of this article.)

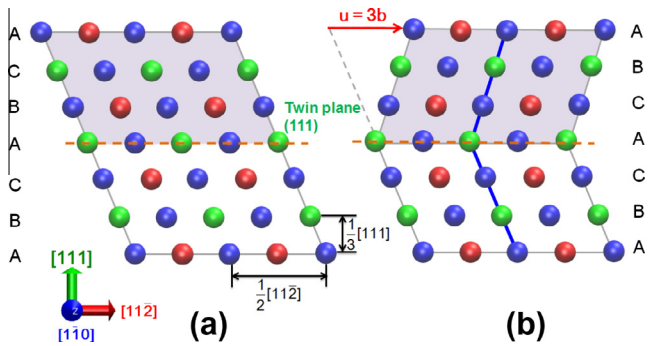

Fig. 4. Deformation twinning in the (1 1 1) plane with partial dislocation 1/6[1 1 $\bar{2}$] (Burgers vector **b** = 1.45 Å) of $L1_0$ Ni_2FeGa. (a) The perfect $L1_0$ lattice viewed from the [1 $\bar{1}$ 0] direction. Twining plane (1 1 1) is indicated by a brown dashed line. (b) The lattice with a three layer twin after shearing along the 1/6[1 1 $\bar{2}$] dislocation *u*, shown by a red arrow. (For interpretation of the references to color in this figure legend, the reader is referred to the web version of this article.)

is marked with the brown dashed line). The atomic arrangement is viewed in the [1 $\bar{1}$ 0] direction. We note that the stacking sequence ABCABCA... in the perfect lattice changed to ABCACBA... in the three layer twin (i.e. plane B moves to the position of plane C after generation of a one layer twin, and plane C moves to the position of plane B when a two layer twin is created).

In Fig. 5 the shear displacement in each successive plane (1 1 1) *u* is normalized to the respective required Burgers vector **b** = 1.45 Å along the [1 1 $\bar{2}$] direction. We define γ_{us} as the stacking fault nucleation barrier, which is the barrier preventing a one layer partial fault from becoming a one layer full fault, γ_{isf} as the first layer intrinsic stacking fault energy (SFE), γ_{ut} as the twin nucleation barrier, which is the barrier against a one layer partial fault becoming a two layer partial fault, and $2\gamma_{tsf}$ as twice the twin SFE [4,12]. Note that γ_{us} and γ_{ut} cannot be experimentally measured and must be computed [12]. The twin migration energy is denoted by $\gamma_{TM} = \gamma_{ut} - 2\gamma_{tsf}$ (shown by the vertical green arrow in Fig. 5), which is most relevant in the presence of existing twins and determines the twin migration stress [5]. Table 1 summarizes the calculated fault energies for twin system 1/6[1 1 $\bar{2}$](1 1 1) of $L1_0$ Ni_2FeGa and for twin system 1/7[1 0 0](0 1 0) of 14M Ni_2FeGa (twinning in 14M will be discussed in the next section). We will see in the next section that the critical twin nucleation stress τ_{crit} for $L1_0$ Ni_2FeGa strongly depends on these fault energies and barriers. Thus utilizing ab initio DFT to precisely establish the GPFE landscape is essential in computing τ_{crit}.

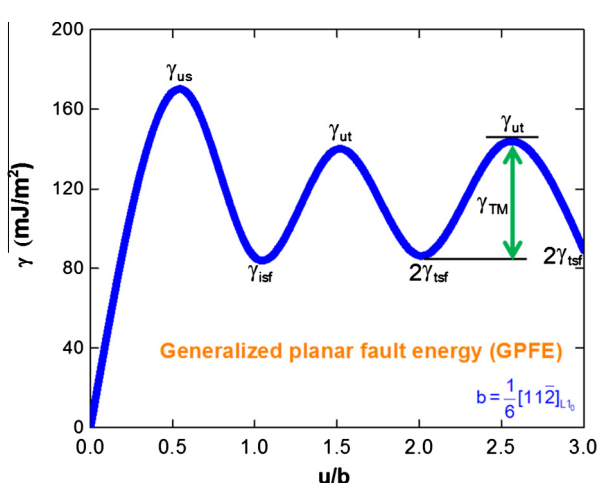

Fig. 5. GPFE in the (1 1 1) plane with a 1/6[1 1 $\bar{2}$] twinning dislocation of $L1_0$ Ni_2FeGa. The calculated fault energies are shown in Table 1.

2.3. Twinning energy landscapes (GPFE): the 14M Ni_2FeGa example

Experiments have shown that Ni_2FeGa alloys exhibit phase transformations from the austenite $L2_1$ (cubic) to intermartensite 10M/14M (modulated monoclinic), and martensite $L1_0$ (tetragonal) phases [35–37]. Modulated monoclinic 14M is an internally twinned long period stacking order structure, which can be constructed from a $L2_1$ cubic structure by a combination of shear (distortion) and atomic shuffling [38] (Fig. 6a and b). Twinning system (1 1 0)[1 $\bar{1}$ 0] in the austenite $L2_1$ coordinates has been observed for the 14M structure [39–41] (Fig. 6c), which corresponds to (0 1 0)[1 0 0] in the 14M coordinates. Fig. 6c shows the internally twinned 14M structure, and Fig. 6d is the detwinned structure after shearing in certain $(1\,1\,0)_{L21}$ planes. To establish the GPFE curve for twinning in 14M we first calculated the lattice parameters and monoclinic angle of 14M. We constructed a supercell containing 56 atoms to incorporate the full period of modulation in the 14M supercell [42,43]. The initial calculation parameters and the monoclinic angle were estimated by assuming lattice correspondence with the 10M structure [35,38,44–46]. The calculated lattice parameters $a_{14M} = 4.24$ Å, $b_{14M} = 5.38$ Å and $c_{14M} = 4.181$ Å and monoclinic angle $\beta = 93.18°$ are in excellent agreement with the experimental data [35]. Fig. 7 shows the calculated GPFE curve of 14M, and the calculated fault energies for twin system 1/7[1 0 0](0 1 0) are summarized in Table 1.

3. Twin nucleation model based on the P–N formulation: the $L1_0$ Ni_2FeGa example

It has been experimentally observed that the morphology of the twinning dislocations array near the twin tip is thin and semi-lenticularly shaped [47–50]. The critical stage of twin nucleation is activation of the first twinning partial

Table 1
Calculated fault energies (mJ m^{-2}) for twin system 1/6[1 1 $\bar{2}$](1 1 1) of $L1_0$ Ni_2FeGa and 1/7[1 0 0](0 1 0) of 14M Ni_2FeGa.

Material	Twin system	γ_{us}	γ_{isf}	γ_{ut}	$2\gamma_{tsf}$	γ_{TM}
$L1_0$ Ni_2FeGa	1/6[1 1 $\bar{2}$](1 1 1)	168	85	142	86	56
14M Ni_2FeGa	1/7[1 0 0](0 1 0)	87	49	83	49	34

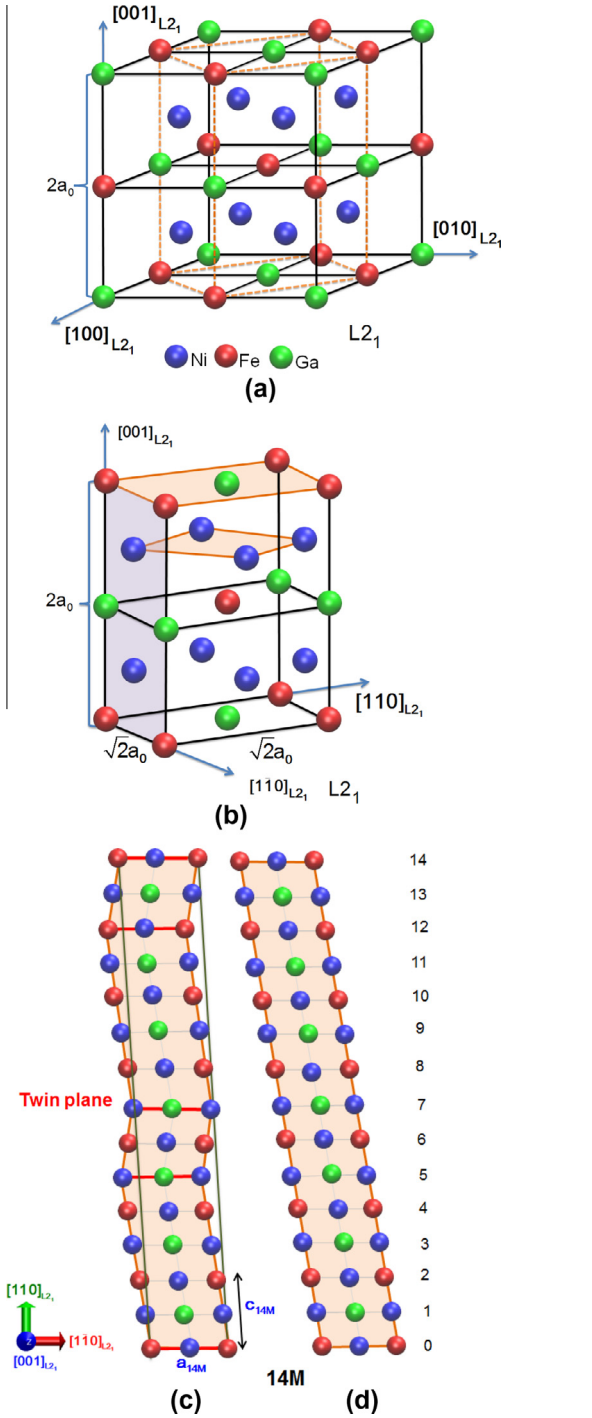

Fig. 6. Crystal structures of modulated monoclinic 14M (internally twinned) and detwinned 14M of Ni_2FeGa. Like the modulated monoclinic 10M structure, 14M can be consructed from a $L2_1$ cubic structure by a combination of shear (distortion) and atomic shuffle [36]. (a) Schematic of the $L2_1$ cubic structure of Ni_2FeGa. (b) The sublattice of $L2_1$ (fct structure) displaying the modulated plane $(1\,1\,0)_{L21}$ (violet) and basal plane $(0\,0\,1)_{L21}$ (brown). (c) The modulated monoclinic 14M (internally twinned) structure with twin plane $(1\,1\,0)_{L21}$ and twin direction $[1\,\bar{1}\,0]_{L21}$. Note the twin system $(1\,1\,0)$ $[1\,\bar{1}\,0]$ in the austenite $L2_1$ coordinates corresponds to $(0\,1\,0)[1\,0\,0]$ in the intermartensite 14M coordinates. (d) The detwinned 14M structure. (For interpretation of the references to color in this figure legend, the reader is referred to the web version of this article.)

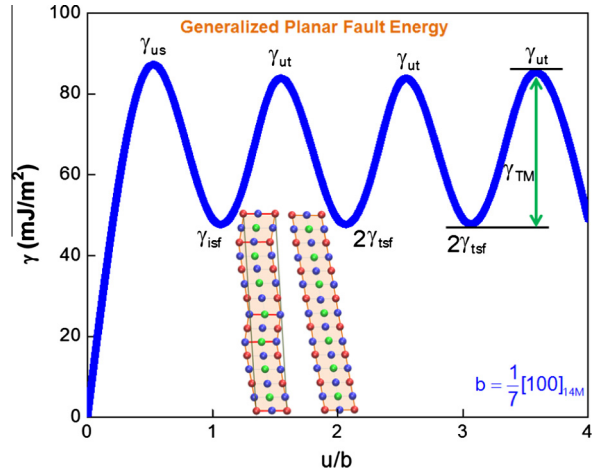

Fig. 7. GPFE in the $(0\,1\,0)$ plane with $1/7[1\,0\,0]$ twinning dislocation of 14M Ni_2FeGa. The calculated fault energies are shown in Table 1.

dislocation on the twin plane involving an intrinsic stacking fault [47,50–52]. This can occur in a region of high stress concentration, such as inclusions, grain boundaries, and notches [51]. Fig. 8 is a schematic illustration of the twin morphology with twinning plane $(1\,1\,1)$ and twinning partial $1/6[1\,1\,\bar{2}]$ in $L1_0$ Ni_2FeGa. h is the twin thickness, N is the number of twin layers, and d is the spacing between two adjacent twinning dislocations and varies depending on their locations relative to the twin tip. It has been experimentally observed that twinning partials near the twin tip are more closely spaced (d is smaller) than dislocations far from the twin tip (d is larger) [47]. τ is the applied shear stress and the minimum τ to form a twin is termed the critical twin nucleation stress τ_{crit}. Once the first twinning partial (leading twinning dislocation) has nucleated, subsequent partials readily form on successive twin planes [52]. We note that a three layer fault forms the twin nucleus in $L1_0$ Ni_2FeGa, which reproduces the $L1_0$ structure. Thus the number of twin layers N is 3 and we seek to minimize the total energy as described below.

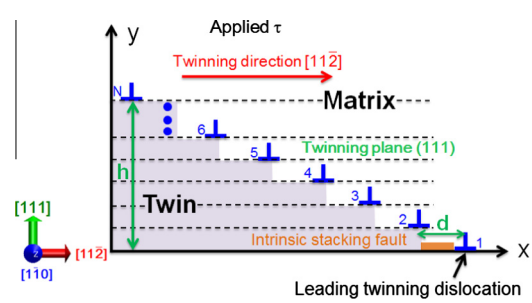

Fig. 8. Schematic illustration showing the semi-lenticular twin morphology of $L1_0$ Ni_2FeGa, viewed in the $[1\,\bar{1}\,0]$ direction. The twinning plane is $(1\,1\,1)$ and twinning direction is $[1\,1\,\bar{2}]$. h is the twin thickness and N is the number of twin layers ($N = 3$ for twin nucleation). d is the spacing between two adjacent twinning dislocations and is considered to be constant for a three layer twin.

The total energy associated with the twin nucleation shown in Fig. 8 can be expressed as:

$$E_{total} = E_{int} + E_{GPFE} + E_{line} - W \tag{1}$$

where E_{int} is the twin dislocation interaction energy, E_{GPFE} is the twin boundary energy (GPFE), E_{line} is the twin dislocation line energy and W is the applied work. These energy terms can be described as follows.

3.1. Twinning dislocations interaction energy E_{int}

The energy for the ith twinning dislocation interacting with the $(i+n)$th or $(i-n)$th dislocation is [53,54]

$$E_{i,i+n/i-n} = \frac{\mu b^2}{4\pi(1-\nu)}(1-\nu\cos^2\theta)\ln\frac{L}{nd} \tag{2}$$

where μ is the shear modulus of the twinning system, **b** is the Burgers vector of the twinning dislocations, ν is the Poisson's ratio, θ is the angle between the Burgers vector and the dislocation line, and L is the dimensions of the crystal containing the twin. After summing for all twinning dislocations we have the energy for the ith dislocation as [53,54]:

$$E_i = \frac{\mu b^2}{4\pi(1-\nu)}(1-\nu\cos^2\theta)\left[\sum_{n=1}^{n=N-i}\ln\frac{L}{nd} + \sum_{m=1}^{m=i-1}\ln\frac{L}{md}\right] \tag{3}$$

where N is the number of layers in the twin nucleus.

The total interactions energy of all twinning dislocations is:

$$E_{int} = \frac{\mu b^2}{4\pi(1-\nu)}(1-\nu\cos^2\theta)\left\{N^2\ln\frac{L}{d} - \left[\ln(n-2)! + \sum_{i=2}^{m=N-1}\ln(N-i)! + \ln(i-1)!\right]\right\} \tag{4}$$

3.2. Twin boundary energy (GPFE) E_{GPFE}

Considering the interaction of multiple twinning dislocations, the disregistry function $f(x)$ can be described by Eq. (5), while Fig. 9 shows a schematic of the normalized $f(x)/\mathbf{b}$ variation with x/ζ. ζ is defined as the half-width of the dislocation for an isotropic solid [55].

$$f(x) = \frac{b}{2} + \frac{b}{N\pi}\left\{\tan^{-1}\left(\frac{x}{\zeta}\right) + \tan^{-1}\left(\frac{x-d}{\zeta}\right) + \tan^{-1}\left(\frac{x-2d}{\zeta}\right) + \cdots + \tan^{-1}\left[\frac{x-(N-1)d}{\zeta}\right]\right\} \tag{5}$$

In the GPFE curve the energy required to create an intrinsic stacking fault can be expressed as:

$$\gamma_{SF}(f(x)) = \gamma_{isf} + \left(\frac{\gamma_{us}-\gamma_{isf}}{2}\right)\left\{1-\cos\left[2\pi\frac{f(x)}{b}\right]\right\} \quad \text{for } 0 \leqslant f(x) \leqslant b \tag{6}$$

The energy required to nucleate a twin can be expressed as:

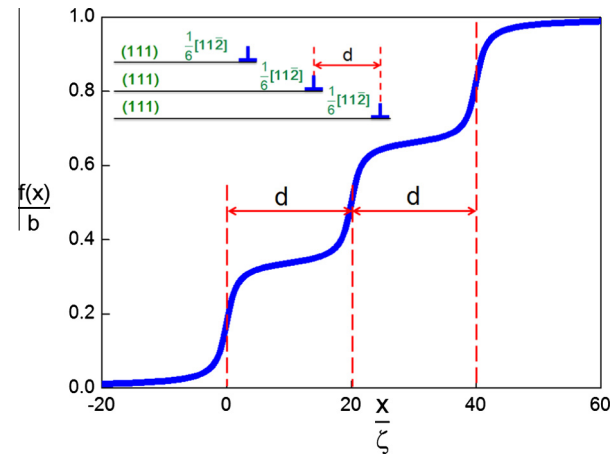

Fig. 9. The disregistry function for three layer twin nucleation ($N = 3$).

$$\gamma_{twin}(f(x)) = \left(\frac{2\gamma_{tsf}+\gamma_{isf}}{2}\right) + \frac{1}{2}\left[\gamma_{ut} - \left(\frac{2\gamma_{tsf}+\gamma_{isf}}{2}\right)\right] \times \left\{1-\cos\left[2\pi\frac{f(x)}{b}\right]\right\} \quad \text{for } b < f(x) \leqslant Nb \tag{7}$$

Thus the twin boundary energy E_{GPFE} can be expressed as:

$$E_{GPFE}(d) = \sum_{m=-\infty}^{+\infty}\gamma[f(mb-d)]b = \sum_{m=-\infty}^{+\infty}\gamma_{SF}[f(mb-d)]b + (N-1)\sum_{m=-\infty}^{+\infty}\gamma_{twin}[f(mb-d)]b \tag{8}$$

3.3. Dislocation line energy E_{line}

$$E_{line} = N\left[\frac{\mu b^2}{2(1-\nu)}(1-\nu\cos^2\theta)\right] = \frac{N\mu b^2}{2(1-\nu)}(1-\nu\cos^2\theta) \tag{9}$$

We will see in the total energy expression that the dislocation line energy E_{line} does not depend on the spacing d, so it will not contribute to the critical twin nucleation stress.

3.4. Applied work W

Assuming the applied stress τ is uniform within the twin, the work done by the applied shear stress on the crystal is:

$$W = N\tau dsh \tag{10}$$

where s is the twinning shear.

When all the terms in the total energy expression are determined the total energy for twin nucleation can be expressed as:

$$E_{total} = E_{int} + E_{GPFE} + E_{line} - W = \frac{\mu b^2}{4\pi(1-\nu)}(1-\nu\cos^2\theta) \times \left\{ N^2 \ln\frac{L}{d} - \left[\ln(N-2)! + \sum_{i=2}^{m=N-1} \ln(N-i)! + \ln(i-1)! \right] \right\} + \sum_{m=-\infty}^{+\infty} \gamma_{SF}[f(mb-d)]b + (N-1)\sum_{m=-\infty}^{+\infty} \gamma_{twin}[f(mb-d)]b + \frac{N\mu b^2}{2(1-\nu)}(1-\nu\cos^2\theta) - N\tau dsh \quad (11)$$

For a constant value of N in specific twin systems the total energy is a function of the spacing between adjacent twinning partials d. The equilibrium d corresponds to the minimum total energy. To determine the critical twin nucleation stress τ_{crit} we minimized the total energy for twin nucleation E_{total} with respect to d:

$$\frac{\partial E_{total}}{\partial d} = 0 \quad (12)$$

The derived explicit and closed form expression for τ_{crit} is given by:

$$\tau_{crit} = \frac{\mu b^2(1-\nu\cos^2\theta)N}{4\pi(1-\nu)shd} + \frac{b}{N^2 sh}\left\{ \gamma_{us} - \gamma_{isf} + (N-1)\left[\gamma_{ut} - \left(\frac{2\gamma_{tsf} + \gamma_{isf}}{2} \right) \right] \right\} \times \sum_{m=-\infty}^{m=\infty} \sin\left\{ \frac{2}{N}\left[\tan^{-1}\left(\frac{mb-d}{\zeta}\right) + \cdots + \tan^{-1}\left(\frac{mb-Nd}{\zeta}\right) \right] \right\} \times \left[\frac{-\zeta}{\zeta^2 + (mb-2d)^2} + \cdots + \frac{-(N-1)\zeta}{\zeta^2 + (mb-Nd)^2} \right] \quad (13)$$

We compared the critical twin nucleation stress τ_{crit} for $L1_0$ and 14M Ni_2FeGa predicted from our P–N formulation based twin nucleation model with the experimental twinning stress data, and found excellent agreement without any fitting parameters (Table 2). The "ideal twinning stress" is calculated from the maximum slope of the GPFE curve with respect to the shear displacement and in the form $\tau_{TMideal} = \pi\{\frac{\gamma_{TM}}{b}\}$ [4]. Based on the P–N model shown in the Appendix [4] the "Peierls stress τ_p" needed to move a twin partial dislocation was also determined. Note that in Eq. (A4) $\gamma_{\max}$ is replaced by γ_{TM}. We note that the ideal twinning stress of 1420 MPa for $L1_0$ is an order of magnitude larger than the twin nucleation stress observed experimentally. Even though the Peierls stress of 230 MPa is smaller than the ideal twinning value, it is still much larger than experimental value of 35–50 MPa. Similarly, for 14M the ideal twinning stress and Peierls stress are much larger than the experimental values. Our model shows favorable agreement between the experimental data and the theory for 14M (27.5 MPa experiment (our experiment) vs. 30 MPa theory (Eq. (13))). This observation demonstrates that the P–N formulation based twin nucleation model provides an accurate prediction of the twin nucleation stress.

Table 2
The predicted critical twin nucleation stress τ_{crit} is compared with ideal twinning stress $\tau_{TMideal}$, Peierls stress τ_p, and available experimental data in $L1_0$ and 14M Ni_2FeGa.

Ni_2FeGa crystal structure	Twin stress (MPa)			
	Ideal[a]	Based on Peierls[b]	This study[c]	Experimental [32]
$L1_0$	1420	230	52	35–50
14M	1779	120	30	25–35

[a] $\tau_{TMideal} = \pi\{\frac{\gamma_{TM}}{b}\}$.
[b] $\tau_p = \max\left\{\frac{1}{b}\frac{E_i^{TM}(u)}{du}\right\}$.
[c] τ_{crit} Eq. (13).

We note that in the energy expressions the spacing between the first (leading) and the second dislocation d, i.e. the tip behavior or the first two layers, governs the results. Therefore, the effect of varying the spacing d along the length of the twin was considered, but this modification did not change the stress values obtained in this work (the stress values calculated by varying the equilibrium spacing and by assuming constant equilibrium spacing were within 5%). For example, values of 3.8, 49, and 126 MPa, respectively, were obtained for Ni_2MnGa 10M, Ni_2FeGa $L1_0$ MPa and NiTi[3] B19′ with variable d values, in comparison with 3.5, 51 and 129 MPa, respectively, for constant d values.

4. Prediction of twinning stress in shape memory alloys

To validate the P–N formulation based twin nucleation model we calculated the critical twinning stress τ_{crit} predicted from the model for several important shape memory alloys and compared the results with experimental twinning stress data. The martensitic crystal structures of these materials were 10M (five layered modulated tetragonal structure for Ni_2MnGa and five layered modulated monoclinic structure for Ni_2FeGa), 14M (seven layered modulated monoclinic structure), $L1_0$ (non-modulated tetragonal structure) and B19′ (monoclinic structure). We found excellent agreement between the predicted values and the experimental data without any fitting parameters in theory, as shown in Table 3. The equilibrium d corresponding to the minimum total energy for different materials is also shown in Table 3. We considered both the important crystal structures 10M and 14M in Ni_2MnGa and the monoclinic B19′ structure of NiTi. In all cases we determined the lattice constants prior to our simulations. The twin system and unstable twin nucleation energy γ_{ut} corresponding to SMAs are also given.

We plot the predicted and experimental twinning stress of the SMAs considered here against γ_{ut} in Fig. 10. We note a monotonic increase in twinning stress with γ_{ut}, which, for the first time, establishes an extremely important correlation between τ_{crit} and γ_{ut} in SMAs. A similar correlation between τ_{crit} and γ_{ut} has been observed for fcc metals

Table 3
Predicted critical twin nucleation stresses τ_{crit}^{theory} for shape memory alloys are compared with known reported experimental values τ_{crit}^{expt}.

Material	Twin system	γ_{ut} (mJ m^{-2}) (predicted)	d (Å) (predicted)	τ_{crit}^{theory} (MPa)	τ_{crit}^{expt} (MPa)
Ni_2MnGa 10M	[100](010)	11	38	3.5	0.5–4 [56–62]
Ni_2MnGa 14M	[100](010)	20	21	9	2–10 [40,60]
NiTi[1] B19′	(001)[100]	25	45	20	20–28 [5,63]
Co_2NiGa $L1_0$	(1 1 1)[1 1 $\bar{2}$]	41	42	26	22–38 [28,64]
Ni_2FeGa 14M	[100](010)	87	17	30	25–40 [15,35]
NiTi[2] B19′	(100)[001]	102	35	43	26–47 [5,63]
Co_2NiAl $L1_0$	(1 1 1)[1 1 $\bar{2}$]	124	37	48	32–51 [64,65]
Ni_2FeGa $L1_0$	(1 1 1)[1 1 $\bar{2}$]	142	24	51	35–50 [15,35]
NiTi[3] B19′	(2 0 $\bar{1}$)[$\bar{1}$ 0 $\bar{2}$]	180	9	129	112–130 [5,18]

The twin systems, equilibrium spacing d and unstable twin nucleation energy corresponding to SMAs are given (10M, 14M, $L1_0$ and B19′ are the martensitic crystal structures explained in the text).

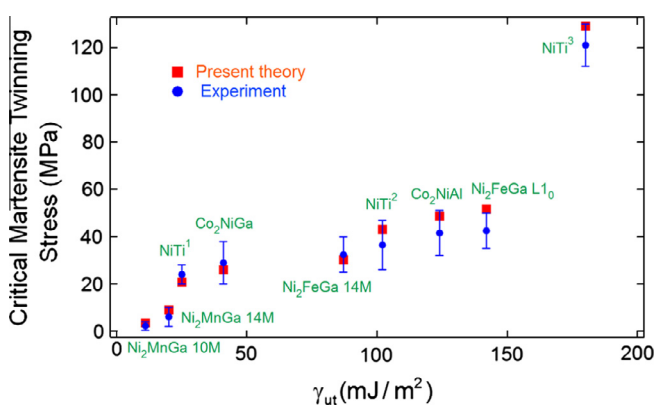

Fig. 10. The predicted and experimental twinning stress for SMAs versus unstable twin nucleation energy γ_{ut}, from Table 3. The predicted twinning stress (red squares) is in excellent agreement with the experimental data (blue circles). The P–N formulation based twin nucleation model reveals an overall monotonic trend between τ_{crit} and γ_{ut}. Note that NiTi[1], NiTi[2] and NiTi[3] indicate three different twinning systems in NiTi, as shown in Table 3. (For interpretation of the references to color in this figure legend, the reader is referred to the web version of this article.)

[12]. The physics of twinning indicates that in order to form a twin boundary and for layer by layer growth to the next twinning plane the twinning partials must overcome the twin nucleation barrier γ_{ut}. However, the relationship is affected by other parameters in the model, so both the model and experimental data point to a rather complex relationship.

5. Determination of twinning stress from experiments

In an earlier work we experimentally determined the critical martensite twinning stress for the shape memory alloys Ni_2MnGa, Ni_2FeGa and NiTi (the Ni_2MnGa data was unpublished), which is reported here. Fig. 11 shows the critical martensite twinning stress vs. temperature for the fully martensitic phase of Ni_2MnGa 10M, Ni_2FeGa 14M, Ni_2FeGa $L1_0$, and NiTi B19′. We note that the twinning stress levels are nearly temperature independent in the martensite regime, as shown. The experimental stress levels are shown for the martensitic regime only, and different alloys have different martensite finish temperatures. To ensure fully martensitic microstructure our experiments were conducted near −200 °C in some cases.

A set of stress–strain experiments was conducted on Ni_2FeGa. The typical compressive stress–strain curve of Ni_2FeGa 14M at −190 °C, which is below the martensite finish temperature (M_f), is shown in Fig. 12 (this curve is representative of five repeated experiments). The experiments were conducted in compression loading of [0 0 1] oriented single crystals of $Ni_{54}Fe_{19}Ga_{27}$. For $T < M_f$ the crystal is in the 14M state [15] subsequent to detwinning and reorientation when the loading reached the critical twinning stress of 55 MPa. Because the Schmid factor for the compressive axis [0 0 1] and twin system $\{1\ 1\ 0\}\langle 1\ \bar{1}\ 0\rangle$ in Ni_2FeGa 14M is 0.5, the critical twinning stress at a temperature of −190 °C was 27.5 MPa. This experimentally measured twinning stress is in excellent agreement with the predicted value from the P–N formulation based twin nucleation model (30 MPa based on Eq. (13)). Upon unloading the twinning-induced deformation remains as "plastic" strain. However, If the material is heated above the austenite finish temperature (A_f) martensite to austenite transformation occurs and the "plastic" strain can be fully recovered (shown by the blue arrow).

6. Discussion of the results

We have presented a general framework for describing twinning in shape memory materials with attention to the

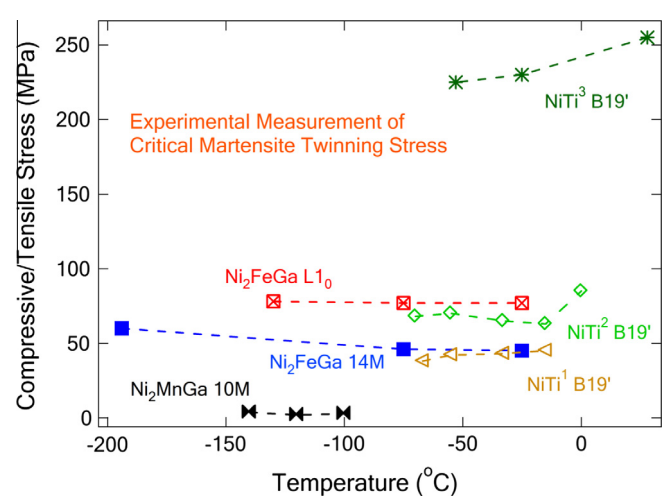

Fig. 11. The critical martensite twinning stress from deformation experiments conducted by Sehitoglu's group. The materials are in the fully martensitic phase of Ni_2MnGa 10M, Ni_2FeGa 14M and $L1_0$, and NiTi B19′. NiTi[1], NiTi[2] and NiTi[3] indicate three different twinning systems in NiTi, as shown in Table 3. Note that the critical stress is nearly temperature independent.

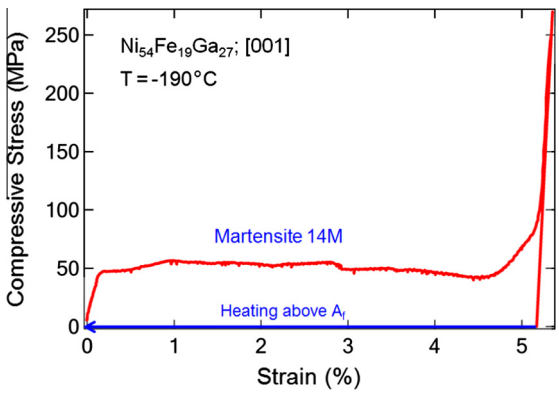

Fig. 12. Compressive stress–strain response of $Ni_{54}Fe_{19}Ga_{27}$ at a constant temperature of −190 °C.

processes on the atomistic scale. Inevitably, the twinning of monoclinic, tetragonal, modulated monoclinic and orthorhombic martensitic structures is complex. This paper tries to demonstrate this complexity and revises the original P–N model. Without such an understanding the characterization and design of new shape memory systems do not have a strong scientific basis. We suggest that the results could serve as the foundation to develop a shape memory materials modeling and discovery methodology, where the deformation behavior of the material at the atomic level directly using quantum mechanics informs the higher length scale calculations. This methodology incorporates the mesoscale P–N calculation. Previously we showed how energy barriers (calculated using first-principles DFT) are utilized in fcc metals to capture the twinning stress. We note added complexities in the ordered shape memory alloys, and the need to understand the mechanisms of complex twinning where shear and relaxation of atoms lead to accurate GPFE descriptions. We note that the magnitude of the Peierls stress calculated from the "classical" Peierls–Nabarro model depends exponentially on the dislocation core size, and therefore the model predicts significant core size dependence of critical stress nearly an order of magnitude [4,25,38]. However, the derived formula for critical twin nucleation stress in the present study does not have this exponential form, and the stress is dependent on the elastic strain energy due to the interaction of twinning partials, in addition to the misfit energy. Therefore, the dislocation core size affects the twinning stress only slightly. For example, for $L1_0$ Ni_2FeGa varying ζ in the range 1–1.5 Å ($\theta = 0$–$90°$) resulted in τ_{crit} values in the range 49–51 MPa. We also performed calculations using the local density approximation (LDA) to determine the planar fault energies and performed simulations with the modified fault energies. The results are in agreement within 15% in most cases (for example the γ_{isf} values were 89 and 85 mJ m^{-2} and γ_{ut} levels were 153 and 142 mJ m^{-2} for the LDA and GGA, respectively). The GGA based results compare more favorably with the experimental twin stress levels.

The modeling results were checked against selected experiments to test the capability of the methodology proposed. The simulations were undertaken on new shape memory alloys such as Ni_2FeGa, Co_2NiAl and Ni_2MnGa exhibiting low twinning stresses (<50 MPa). This is in addition to the more established but equally complex NiTi, which has multiple twin modes with higher twin stresses (reaching >150 MPa). We further verified the predictions with experiments measuring the twinning stress in 14M (modulated monoclinic) Ni_2FeGa, with excellent agreement.

There are several observations that are unique to the findings in this study. We note that twinning in these alloys cannot be classified with as a simple mirror reflection; the shuffling due to relaxation at the interfaces needs to be considered. This modification provides more accurate energy barriers. In addition to establishing the twinning stress, our study provides a wealth of information, such as the lattice constants (and hence the volume change, which plays an important role in shape memory alloys) and the shear moduli, which can all be measured experimentally.

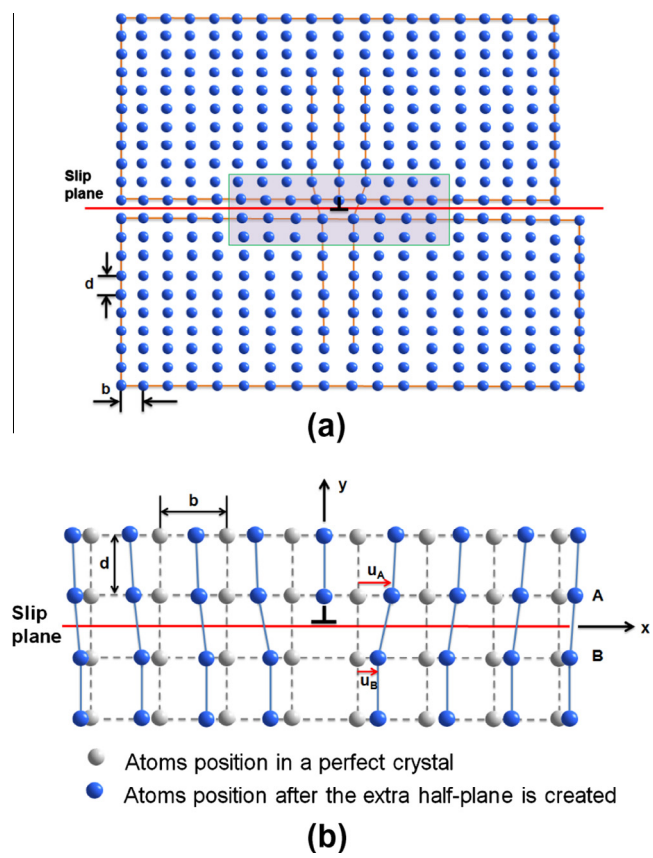

Fig. A1. (a) Configuration of the Peierls–Nabarro model for dislocation slip. b is the lattice spacing along the slip plane and d is the lattice spacing between adjacent planes. (b) The enlarged configuration of the green box in (a). The gray and blue spheres represent the atom positions before and after the extra half-plane is created. $u_A(x)$ and $u_B(x)$ are the atom displacements above the slip plane (on plane A) and below the slip plane (on plane B), and their difference $u_A(x) - u_B(x)$ describes the disregistry distribution $f(x)$ as a function of x. (For interpretation of the references to color in this figure legend, the reader is referred to the web version of this article.)

Determination of the twinning stress is far more difficult experimentally, because the experiments need to be performed well below room temperature in several cases and very precise stress–strain curves measurements on samples with uniform gage sections need to be established.

Significant effort has been devoted to lowering the magnitude of twinning stress in magnetic shape memory (MSM) alloys. The main alloy system studied has been Ni_2MnGa, because it undergoes twinning at stress levels of <10 MPa. The other candidate alloys of interest include Ni_2FeGa, Co_2NiAl, and Co_2NiGa. Their twinning stress levels are also rather low (<30 MPa). We can predict the twinning stress in these materials with considerable accuracy and without the need for adjustable constants. NiTi is a complex system because the twin modes change with deformation, from the {0 0 1} system to the {0 1 2} and higher order ones. This results in an overall higher twin stress in the case of NiTi.

Finally, we note that in the "pseudoelasticity" case, when the SMA undergoes isothermally stress-induced transformation from austenite to martensite, martensite undergoes detwinning and this contributes to the overall recoverable strain. Upon unloading martensite reverts back to austenite, termed "pseudoelasticity". The magnitude of the correspondence variant pair formation strain is of the order of 5% in NiTi while the shear associated with detwinning is also nearly 5%, making the total near 10%. In the case of Ni_2FeGa the magnitudes of the strains are higher (near 14%), and the process of twinning plays a considerable role [13]. It is difficult to determine the twinning stress during pseudoelasticity experiments, therefore, theoretical calculations such as presented in this paper provide a significant understanding.

7. Conclusions

This work supports the following conclusions.

(1) The proposed twin nucleation model shows that Ni_2MnGa 10M undergoes twinning at a stress level as low as 3.5 MPa, in agreement with the experiment reults (<4 MPa). Ni_2FeGa 14M undergoes twinning at 30 MPa, also in very close agreement with the experiments conducted in this study (27.5 MPa). The predicted twinning stresses for NiTi are higher (43 MPa for the (1 0 0) case and 129 MPa for the $(2\,0\,\bar{1})$ case), also in close agreement with the experimental data.

(2) The twinning stress for the newly proposed ferromagnetic SMAs Co_2NiGa, Co_2NiAl are 26 and 48 MPa, respectively, also in close agreement with experiments (22–38 MPa for Co_2NiGa and 32–51 MPa for Co_2NiAl).

(3) Depending on the martensitic structure and twin systems, the twinning processes may involve combined shear and atomic shuffling, as in the case of B19′ NiTi (1 0 0), which makes determination of the GPFE landscape challenging. Nevertheless, determination of the out-of-plane displacements at twin interfaces during simulations provides increasingly accurate results for the energy barriers.

(4) The proposed twin nucleation model reveals that τ_{crit} has an overall monotonic dependence on the unstable twin nucleation energy γ_{ut}. The τ_{crit} vs. γ_{ut} plot was chosen to compare theory with experiment. We note that τ_{crit} prediction depends on the entire GPFE landscape, the elastic constants, and the Burgers vectors, so a simple relationship cannot be written in an algebraic form. To achieve lower twinning stresses in SMAs shorter Burgers vectors, lower unstable twin energies and larger interplanar distances are desirable.

Acknowledgement

The work was supported by a graduate fellowship (J.W.).

Appendix A. Peierls–Nabarro model fundamentals

The Peierls–Nabarro model considers two semi-infinite continuous half crystals joined at the slip plane with a dislocation inserted [66]. The behavior of the half crystals is confined to linear elasticity and all non-linear behavior is confined to a single plane, as shown in Fig. A1 [67].

According to the P–N model the total energy of the dislocation with the two half crystals in Fig. A1 can be expressed as [66]:

$$\begin{aligned} E_{tot} &= E_{elast} + E_{mis} \\ &= \frac{-K}{4\pi}\int_{-\infty}^{\infty}\int_{-\infty}^{\infty}\frac{df(x)}{dx}\frac{df(x')}{dx'}\ln|x-x'|dxdx' \\ &\quad + \lim_{R\to\infty}\frac{Kb^2}{4\pi}\ln R + \int_{-\infty}^{\infty}\gamma[f(x)]dx \end{aligned} \tag{A1}$$

where E_{elast} accounts for the elastic strain energy stored in the two half crystals, while E_{mis} is the misfit energy representing the non-linear interatomic interactions in the dislocation core and depends on the position of the dislocation line within a lattice cell and, hence, is periodic [4,55,68]. The parameter K is a material property measuring the elastic response of the lattice to displacement along the Burgers vector direction [55], and γ is the generalized stacking fault energy representing the fault energy associated with dislocation motion [3,46].

By considering the lattice discreteness the misfit energy E_{mis} can be defined as the sum of all the misfit energies between pairs of atom rows as a function of u [22,66]:

$$E_{mis}(u) = \sum_{m=-\infty}^{+\infty}\gamma[f(ma'-u)]a') \tag{A2}$$

where a' is the periodicity of $E_{mis}(u)$ and is defined as the shortest distance between two equivalent atomic rows in

the direction of the dislocation displacement [69–71]. The solution of the disregistry function $f(x)$ in the dislocation core is [45,66,71,72]:

$$f(x) = \frac{b}{2} + \frac{b}{\pi}\arctan\left(\frac{x}{\zeta}\right) \tag{A3}$$

where $\zeta = d/[2(1-\nu)]$ is the half-width of the dislocation for an isotropic solid [55], d is the interplanar distance between the twinning planes and ν is the Poisson's ratio. Using the Frenkel expression [66] $\gamma[f(x)]$ can be written as:

$$\gamma[f(x)] = \frac{\gamma_{\max}}{2}\left[1 - \cos\frac{2\pi f(x)}{b}\right] \tag{A4}$$

where $\gamma_{\max}$ is maximum fault energy. After substituting Eqs. (A3) and (A4) into Eq. (A2), we have the following summation form with m as integer:

$$\begin{aligned} E_{\gamma}^{s}(u) &= \sum_{m=-\infty}^{+\infty} \gamma[f(ma' - u)]a' \\ &= \sum_{m=-\infty}^{+\infty} \frac{\gamma_{\max}}{2}\left\{1 + \cos\left[2\tan^{-1}\left(\frac{ma' - u}{\zeta}\right)\right]\right\}a' \end{aligned} \tag{A5}$$

Because the elastic strain energy E_{elast} is independent of the location of the dislocation line u, the Peierls stress τ_p is then given by the maximum stress required to overcome the periodic barrier in $E_{mis}(u)$:

$$\tau_p = \max\left\{\frac{1}{b}\frac{dE_{tot}}{du}\right\} = \max\left\{\frac{1}{b}\frac{dE_{mis}(u)}{du}\right\} \tag{A6}$$

References

[1] Otsuka K, Wayman CM, editors. Shape memory materials. Cambridge: Cambridge University Press; 1998.
[2] Funakubo H. Shape memory alloys. New York: Gordon and Breach; 1987 [translated from the Japanese by J.B. Kennedy].
[3] Vitek V. Philos Mag 1968;18:773.
[4] Ogata S, Ju L, Yip S. Phys Rev B Condens Matter Mater Phys 2005;71:224102.
[5] Ezaz T, Sehitoglu H, Maier HJ. Acta Mater 2011;59:5893.
[6] Nishida M, Ohgi H, Itai I, Chiba A, Yamauchi K. Acta Metall Mater 1995;43:1219.
[7] Zhang JX, Sato M, Ishida A. Acta Mater 2006;54:1185.
[8] Venables JA. Deformation twinning in fcc metals. New York: Gordon and Breach; 1964.
[9] Orowan E. Dislocations and mechanical properties. New York: Institute of Metals Division, The American Institute of Mining and Metallurgical Engineers; 1954.
[10] Armstrong R. Role of deformation twinning in fracture processes. New York: Gordon and Breach; 1964.
[11] Meyers MA, Vohringer O, Lubarda VA. Acta Mater 2001;49:4025.
[12] Kibey S, Liu JB, Johnson DD, Sehitoglu H. Acta Mater 2007;55:6843.
[13] Hamilton RF, Sehitoglu H, Efstathiou C, Maier HJ. Acta Mater 2007;55:4867.
[14] Hamilton RF, Efstathiou C, Sehitoglu H, Chumlyakov Y. Scripta Mater 2006;54:465.
[15] Timofeeva E, Panchenko EY, Chumlyakov YI, Maier H. Russ Phys J 2012:1.
[16] Kresse G, Hafner J. Phys Rev B Condens Matter 1993;48:13115.
[17] Kresse G, Furthmuller J. Phys Rev B Condens Matter 1996;54:11169.
[18] Ezaz T, Sehitoglu H, Abuzaid W, Maier H. Mater Sci Eng 2012;558. p. 442.
[19] Hodgson DE, Ming W, Biermann RJ. In: metals handbook, 10th ed., vol. 2. Materials Park, OH: ASM International; 1990. p. 897.
[20] Fu CL, Yoo MH. Acta Metall Mater 1992;40:703.
[21] Paidar V. Czechoslovak J Phys 1976;26:865.
[22] Juan Y-M, Kaxiras E. Philos Mag 1996;74A:1367.
[23] Whang SH, Feng Q, Gao YQ. Acta Mater 1998;46:6485.
[24] Pond RC, Muntifering B, Müllner P. Acta Mater 2012;60:3976.
[25] Rajasekhara S, Ferreira PJ. Scripta Mater 2005;53:817.
[26] Brown PJ, Dennis B, Crangle J, Kanomata T, Matsumoto M, Neumann K-U, et al. J Phys Condens Matter 2004;16:65.
[27] Han M, Bennett JC, Gharghouri MA, Chen J, Hyatt CV, Mailman N. Mater Charact 2008;59:764.
[28] Kireeva I, Chumlyakov Y, Pobedennaya Z, Kretinina I, Cesari E, Kustov S, et al. Phys Metals Metallogr 2010;110:78.
[29] Chu F, Pope DP. Mater Sci Eng 1993;170A:39.
[30] Heo YU, Lee HC. Mater Trans 2007;48:2546.
[31] Yoo M. J Mater Res 1989;4:50.
[32] Kibey S, Liu J, Johnson D, Sehitoglu H. Appl Phys Lett 2006;89:191911.
[33] Siegel DJ. Appl Phys Lett 2005;87:121901.
[34] Warner D, Curtin W, Qu S. Nat Mater 2007;6:876.
[35] Sutou Y, Kamiya N, Omori T, Kainuma R, Ishida K, Oikawa K. Appl Phys Lett 2004;84:1275.
[36] Hamilton RF, Sehitoglu H, Aslantas K, Efstathiou C, Maier HJ. Acta Mater 2008;56:2231.
[37] Masdeu F, Pons J, Segui C, Cesari E, Dutkiewicz J. J Magn Magn Mater 2005;290–291:816.
[38] Kang K, Bulatov VV, Cai W. Proc Natl Acad Sci 2012;109:15174.
[39] Soolshenko V, Lanska N, Ullakko K. In: International conference on martensitic transformations, June 10–14, 2002, vol. 112 II. Espoo, Finland: EDP Sciences; 2003. p. 947.
[40] Sozinov A, Likhachev A, Lanska N, Ullakko K. Appl Phys Lett 2002;80:1746.
[41] Aaltio I, PhD thesis, Aalto University, Finland; 2011.
[42] Zayak A, Adeagbo WA, Entel P, Buchelnikov VD. Phase Trans 2005;78:259.
[43] Luo HB, Li CM, Hu QM, Kulkova SE, Johansson B, Vitos L, et al. Acta Mater 2011;59:5938.
[44] Kainuma R, Nakano H, Ishida K. Metall Mater Trans A Phys Metall Mater Sci 1996;27A:4153.
[45] Schoeck G. Phys Status Solidi B 2011;248:2284.
[46] Sehitoglu H, Wang J, Maier HJ. Int J Plast 2012;39:61.
[47] Jin Z, Bieler TR. Philos Mag 1995;71A:925.
[48] Zhang L. Philos Mag Lett 1999;79:49.
[49] Müllner P, Romanov A. Acta Mater 2000;48:2323.
[50] Gutkin MY, Ovid'ko I, Skiba N. Phys Solid State 2007;49:874.
[51] Marcinkowski M, Sree Harsha K. J Appl Phys 1968;39:6063.
[52] Appel F, Paul JDH, Oehring M. Gamma titanium aluminide alloys: science and technology. New York: Wiley; 2011.
[53] Cooper R. Acta Met 1966;14:78.
[54] Cooper R. Acta Metall 1965;13:46.
[55] Joós B, Ren Q, Duesbery MS. Phys Rev 1994;50B:5890.
[56] Sozinov A, Likhachev AA, Ullakko K. In: SPIE's 8th annual international symposium on smart structures and materials: Active Materials: Behavior and Mechanics, Newport Beach, CA; 2001, vol. 4333, p. 189.
[57] Straka L, Novák V, Landa M, Heczko O. Mater Sci Eng 2004;374A:263.
[58] Callaway JD, Sehitoglu H, Hamilton RF, Aslantas K, Miller N, Maier HJ, et al. Appl Phys Lett 2006;89:221905.
[59] Chulist R, Sozinov A, Straka L, Lanska N, Soroka A, Lippmann T, et al. J Appl Phys 2012;112:063517.
[60] Soolshenko V, Lanska N, Ullakko K. J Phys IV 2003;112:947.
[61] Müllner P, King A. Acta Mater 2010;58:5242.
[62] Müllner P, Chernenko V, Kostorz G. J Magn Magn Mater 2003;267:325.

[63] Sehitoglu H, Karaman I, Anderson R, Zhang X, Gall K, Maier HJ, et al. Acta Mater 2000;48:3311.
[64] Chumlyakov Y, Kireeva I, Panchenko E, Timofeeva E, Pobedennaya Z, Chusov S, et al. Russ Phys J 2008;51:1016.
[65] Dilibal S, Sehitoglu H, Hamilton R, Maier H, Chumlyakov Y. Mater Sci Eng 2011;528A:2875.
[66] Tadmor EB, Miller RE. Modeling materials: continuum, atomistic and multiscale techniques. Cambridge: Cambridge University Press; 2011.
[67] Hirth JP, Lothe J. Theory of dislocations. New York: McGraw Hill; 1968.
[68] Schoeck G. Phys Rev Lett 1999;82:2310.
[69] Carrez P, Ferré D, Cordier P. Philos Mag 2007;87:3229.
[70] Lu G, Kioussis N, Bulatov VV, Kaxiras E. Philos Mag Lett 2000;80:675.
[71] Joós B, Duesbery MS. Phys Rev Lett 1997;78:266.
[72] Dunand D, Mari D, Bourke M, Roberts J. Metall Mater Trans 1996;27A:2820.